Influence of Cooling Rate on the Thermal Behavior and Solid-State Morphologies of Polyhydroxyalkanoates

Yuping Xie,[1] Isao Noda,[2] Yvonne A. Akpalu[3]

[1]*Department of Chemical and Biological Engineering, Rensselaer Polytechnic Institute, Troy, New York 12180*
[2]*The Procter & Gamble Company, Beckett Ridge Technical Center, West Chester, Ohio 45069*
[3]*Department of Chemistry and Chemical Biology, Rensselaer Polytechnic Institute, Troy, New York 12180*

Received 23 October 2007; accepted 26 February 2008
DOI 10.1002/app.28278
Published online 2 May 2008 in Wiley InterScience (www.interscience.wiley.com).

ABSTRACT: The influence of cooling rates on the thermal behavior and solid-state morphologies of polyhydroxyalkanoates have been investigated. The thermal behavior was studied by differential scanning calorimetry (DSC). The crystal structures (~ Å), lamellar (tens of nanometers), fibrillar (several hundred nanometers), and spherulitic (~ μm) morphologies of poly (3-hydroxybutyrate) (PHB) and the copolymers of poly (3-hydroxybutyric acid-*co*-3-hydroxyvaleric acid) (PHBV) and poly (3-hydroxybutyric acid-*co*-3-hydroxyhexanoic acid) (PHBHx) crystallized under different cooling rates were studied using simultaneous small angle X-ray scattering (SAXS) and wide angle X-ray scattering, simultaneous ultra small angle X-ray scattering (USAXS) and SAXS, and polarized optical microscopy, respectively. The experimental results showed that the lamellar and spherulitic morphologies depended strongly on cooling rates. However, there was little influence of cooling rates on the crystal structures. © 2008 Wiley Periodicals, Inc. J Appl Polym Sci 109: 2259–2268, 2008

Key words: X-ray; thermal properties; morphology; processing

INTRODUCTION

Polyhydroxyalkanoates (PHAs) are biodegradable and thermoplastic polyesters produced by a wide variety of bacteria from renewable resources like corn sugar and oil. PHAs have recently attracted much interest because of their biodegradability and biocompatibility.[1–3] They possess mechanical properties comparable with those of conventional thermoplastics, such as polyethylene and polypropylene.[1,2,4] Therefore, PHAs offer a sustainable, renewable alternative to petroleum-based products while, at the same time, providing equal or better performance.[5] However, they also have some disadvantages, including poor thermal stability,[6–9] narrow processing windows and brittleness[10–12] (especially for poly (3-hydroxybutyrate) (PHB)). These disadvantages can be improved by changing processing conditions,[13,14] by changing their chemical structures[15] (e.g., side chain length) and by adding particles,[16] stabilizers,[11] compatibilizers[17] or plasticizers,[18] all of which can influence the solid-state morphologies. Ultimately a molecular level understanding of structure and properties of PHAs will facilitate control over their properties.

For conventional semicrystalline polymers such as polyethylene and polypropylene, the structure-property relation is not fully understood because the morphology of semicrystalline polymeric materials is highly dependent on the preparation (temperature, pressure, shear rate, cooling rate, etc),[19–21] which in turn influences the properties. The relationships between processing conditions and physical properties (mechanical properties and morphologies) of isotactic polypropylene (iPP) and propylene/ethylene copolymers were explored by Kalay and Bevis.[20,21] Shear-controlled orientation injection molding (SCORIM) results in more pronounced molecular orientation than conventional injection molding, which is consistent with the substantial increase in Young's modulus of moldings produced by SCORIM. The improved mechanical properties of iPP moldings is attributed to shish-kebab morphology developed by the action of shear to the solidifying melt. Iwata et al.[14,22,23] studied the mechanical properties of uniaxially cold-drawn films of PHB and its copolymers. Isothermal melt crystallization of PHAs has been widely studied.[10,13,24] For example, Gunaratne and Shanks[10] studied the crystallization

Correspondence to: Y. Akpalu (akpaly@rpi.edu).
Contract grant sponsor: Department of Energy, Basic Energy Sciences; contract grant number: FG02-06ER46349.
Contract grant sponsor: National Science Foundation, Division of Civil, Mechanical, Manufacturing, and Innovation; contract grant number: CMMI 0600317.

behavior of PHB and its copolymer of PHBV by isothermal crystallization kinetics. They attributed multiple melting peak behavior observed for all polymers to melting–recrystallization–remelting process. Abe et al.[13] studied the solid-state structures and thermal properties of isothermally melt-crystallized films of PHAs. They found that both the long period distance and the lamellar thickness of melt-crystallized PHA films were increased with an increase in the crystallization temperature. The melting temperature of PHA films also increased with an increase in the crystallization temperature. From the relationship between lamellar thickness and melting temperature, it has been concluded that randomly distributed second monomer units except for the 3-hydroxyvaleric acid (HV) unit in copolyesters act as defects of PHB crystal and are excluded from the crystalline lamellae. Although isothermal crystallization of PHAs has been widely studied, investigation of nonisothermal crystallization behavior of PHAs is important during the industrial processes, such as extrusion and molding.[25]

Recently, molecular modeling is being used in conjunction with experimental data to predict structures and properties of polymers. Molecular dynamics (MD) has been used to simulate heat capacity, rheological behavior, and small molecule diffusion characteristics using equilibrium and nonequilibrium MD methods. These simulations were conducted using results from diffraction experiments to provide a molecular level insight into the structure-property relationship for polylactide (PLA) and PHA materials.[26] Spitalsky and Bleha[27] have utilized molecular mechanics calculation to examine the deformation response of regular and irregular conformations of PHB. Sato et al.[4] used quantum chemical calculation as well as infrared and Raman spectroscopy to explore the structure and thermal behavior of PHB and PHBHx. They found that C—H...O=C hydrogen bonding exists between the CH_3 group and the C=O group that combines the two parallel helical structures in PHB and PHBHx, and that the hydrogen bonding plays an important role in their thermal behavior. Sheng et al.[28] employed multiscale micromechanical models (numerical as well as analytical) to calculate the overall elastic modulus of the ''as-processed'' amorphous and semicrystalline polymer-clay nanocomposites and to compute their dependence on the matrix and clay properties as well as internal clay structural parameters. The elastic moduli for those ''as-processed'' nanocomposites predicted by the micromechanical models are in good agreement with experimental data. They showed that quantitative structural parameters extracted from experiment such as X-ray diffraction (XRD) patterns and transmission electron microscopy (TEM) micrographs provide a basis for modeling effective mechanical properties of the clay particle. However, it must be noted that the structural parameters are highly dependent on the processing conditions.

The objective of the work is to study the influence of cooling rates on the thermal behavior and solid-state morphologies of PHAs. Since the properties of PHAs can be affected by structures over multiple length scale, several techniques such as differential scanning calorimetry (DSC), polarized optical microscopy (POM) and X-ray scattering methods will be used to study the effect of cooling rate on the structures and morphologies of PHAs. DSC can be used to study the thermal behavior of polymers and obtain the crystallinity. POM is widely used to study the size, distribution, shape and internal structures of spherulites. Ultra small angle X-ray scattering (USAXS) measurements can provide a detailed description of the effect of crystallization conditions on the mesoscale structure of crystalline aggregates. The organization of lamellar crystals and the characteristics of crystals can be obtained from small angle X-ray scattering (SAXS) and wide angle X-ray scattering (WAXS), respectively. Thus by combining DSC, POM, USAXS, SAXS, and WAXS, we can provide process dependent multiple length scale structural information for the development of multiscale models that predict mechanical properties of PHAs.

EXPERIMENTAL

Sample preparation

PHB of M_w = 690,000 g/mol and M_n = 300,000 g/mol, and the copolymer of poly (3-hydroxybutyric acid-*co*-3-hydroxyvaleric acid) of M_w = 407,000 g/mol and M_n = 185,000 g/mol with 8 wt % HV content (PHB8V) produced by bacteria were purchased from Sigma-Aldrich Chemicals. The copolymer of poly (3-hydroxybutyric acid-*co*-3-hydroxyhexanoic acid) of M_w = 903,000 g/mol with 7.2 mol % hydroxyhexanoic acid (HHx) content (PHBHx) was kindly provided by the Procter and Gamble. Polymer (1.0 g) was dissolved in 100 mL of hot chloroform and filtered under vacuum to remove any insoluble fraction or impurities, then was precipitated in cold methanol (400 mL). The mixture was filtered and then the PHA was washed with methanol. This sample was precipitated in cold *n*-hexane (400 mL), filtered and then washed with *n*-hexane using this same protocol described above. After the PHA was dried in a fume hood for 24 h, it was put into a vacuum oven at room temperature for 2 days. The purified PHA samples thus obtained were used for our experiments unless otherwise specified. This purification process has been used by many researchers.[29–32]

Differential scanning calorimetry

Differential scanning calorimetry (DSC) was performed with a DSC Q100 (TA Instruments). The sample was heated from room temperature to 180°C and soaked for 5 min followed by cooling to −80°C at different cooling rates. The reported melting temperature (T_m) was from the second heating from −80 to 190°C at a rate of 10°C/min. DSC experiments were performed under nitrogen (flow rate of 50 mL/min) using sample sizes of 5.0–15.0 mg. The crystallinity was calculated using $X_c = \Delta H_f/\Delta H^0$, where ΔH^0 is the heat of fusion for perfect PHB crystals (146 J/g[10]), perfect PHB8V crystals (109 J/g[32,33]) or perfect PHBHx crystals and ΔH_f the measured heat of fusion for PHB, PHB8V or PHBHx. The ΔH^0 for PHBHx is about 115 J/g based on the heat of fusions from DSC and X-ray crystallinities from WAXS for PHBHx with 8 mol % HH*x*.[13]

Polarized optical microscopy

Polarized optical microscopy (POM) measurements were performed on film samples sealed between two round glass cover slips at room temperature. An optical microscope (Olympus BX51) coupled to an Insight digital camera was used to characterize the solid-state morphology of film samples (~ 15 μm thick). Before any measurements, samples were first melted at 180°C for 5 min under nitrogen to remove any thermal history, and then cooled to room temperature at different cooling rates. All the melting and cooling procedures were performed on a computer interfaced Instec HCS600V hot stage to minimize sample movement and temperature fluctuations.

X-ray scattering

Simultaneous small angle X-ray scattering (SAXS) and wide angle X-ray scattering (WAXS) measurements were carried out at W. M. Keck Nanostructures Laboratory at University of Massachusetts Amherst using an instrument from the Molecular Metrology, equipped with a focusing multilayer monochromator (Osmic MaxFlux) with λ = 1.542 Å. The beam was collimated with three pinholes. For the small angle detection, a 2-D multiwire detector was used. To record the wide angle profiles, an image plate with a hole in the center was inserted into the beam path. For the wide-angle diffraction studies, the scattering peak of an alumina standard SRM 676 (d_{012} = 3.485 Å) was used for angular calibration. Silver behenate (d_{001} = 58.380 Å) was used for angular calibration of the SAXS measurements. The ''POLAR'' software developed by Stonybrook Technology and Applied Research was used to reduce and analyze the SAXS and WAXS data. The sample-to-detector distance for SAXS measurements and that for WAXS measurements were 1.193 and 0.134 m, respectively. All SAXS data were corrected by detector efficiency calibrated by Fe-55.

Simultaneous ultra-small angle X-ray scattering/small angle X-ray scattering (USAXS/SAXS) measurements were carried out at synchrotron radiation beamline 33-ID at UNICAT, Advanced Photon Source, Argonne National Laboratory. At this beamline, a Bonse-Hart setup allows one to record USAXS scattering curves using a photodiode detector with an angular resolution of 0.0001 $Å^{-1}$ in a q range from 0.0001 to 1.0 $Å^{-1}$. The scattering vector q is a typically used quantity in small angle scattering and relates to the scattering angle (2θ), via the relation $q = (4\pi/\lambda)\sin\theta$, where λ is the X-ray wavelength. The data acquisition time for a scattering curve with 150 data points was typically 15 min per sample. All USAXS/SAXS data were fully corrected for all instrumental effects, including subtraction of blank sample background and photodiode dark current, constant flat background due to incoherent scattering, and desmearing.

The samples had cylinder-like shape with diameter of 6.5 mm and thicknesses of ~ 1 mm. The samples were treated in the same way as those for POM measurements to remove any thermal history.

The SAXS data ($q > 0.03$ $Å^{-1}$) were analyzed in reciprocal space by fitting the data using software of Igor Pro 5.0 to the intensity calculated from a model,[34,35] which is called two-component model. The scattering from semicrystalline polymers could be separated into two components: (1) the discrete scattering due to lamellae in the lamellar stacks in which the contrast is due to the regularly spaced interlamellar amorphous regions between the crystalline lamellae and (2) the diffuse scattering from the amorphous domains outside the lamellar stacks or in isolated lamellae in which the contrast is between amorphous domains and the surrounding crystalline regions. From the intensity profile analysis, the long period (L) and amorphous thickness (l_a) can be obtained. The lamellar thickness (l_c) is thus calculated by $L - l_a$.

The limiting slopes of the USAXS data were obtained by fitting the data using Excel software from 0.00055 to 0.0200 $Å^{-1}$, from 0.0040 to 0.0200 $Å^{-1}$, and from 0.00055 to 0.0200 $Å^{-1}$ for PHB, PHB8V, and PHBHx, respectively.

RESULTS AND DISCUSSION

The DSC curves of PHB (as received) and PHB (purified) samples cooled from melt at 50°C/min are shown in Figure 1. The unpurified sample had two melting peaks, whereas the purified sample had

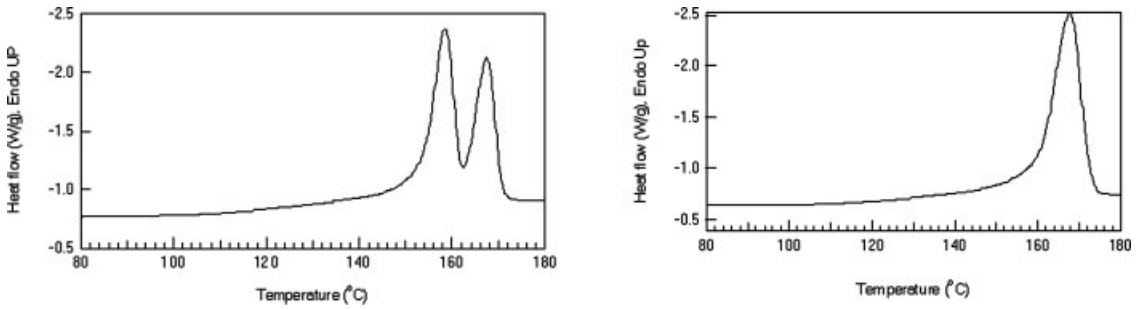

Figure 1 DSC melting curves of PHB (as received) (left) and PHB (purified) (right) cooled from melt at 50°C/min.

only one melting peak. The crystallization behavior of polymers has been widely studied by differential scanning calorimetry (DSC). Double or multiple melting peaks have been reported in isothermally crystallized semicrystalline polymers.[10,36] Possibilities of double or multiple melting behavior are as follows[10]: (1) melting, recrystallization, and remelting during heating, (2) presence of more than one crystal modifications (polymorphism), (3) different morphology (lamellar thickness, distribution, perfection or stability), (4) physical aging or/and relaxation of the rigid amorphous fraction, (5) different molecular weight species and so on. The polydispersities of PHAs studied in this study are about 2 and their glass transition temperatures (T_g's) are less than 6°C,[3,15] so the physical aging or/and relaxation of the rigid amorphous fraction and different molecular weight species are very unlikely to cause the double or multiple melting peaks. Thus for PHBs, the double melting behavior can result from impurities, melting, recrystallization, and remelting during heating, polymorphism or different morphology.

Polarized optical micrographs of PHB (as received) and PHB (purified) samples cooled from melt at 50°C/min are shown in Figure 2. The spherulites of the unpurified sample showed a banded structure, indicating that lamellar twisting exists.[37] In the absence of impurities, a more uniform size distribution and a different spherulitic texture—regular Maltese cross were obtained. In semicrystalline polymers, the banded pattern is very much dependent on the rate of cooling from the melt; the same polymer can show either a simple extinction by itself or a banded pattern in addition as the conditions of crystallization are changed.[37] For example, rapid crystallization of high density polyethylene gives rise to spherulites showing a banded pattern, whereas slow crystallization of the same material gives spherulites with no bands.[38] In the case of linear low density polyethylene, however, rapidly cooled material has a normal extinction cross whereas slowly cooled material shows concentric bands.[37] Thus the impurities in PHBs have a similar effect on the spherulitic morphology as cooling rate.

Thus, to investigate the influence of cooling rate on thermal behavior and morphologies of PHAs, studies on purified samples are required.

DSC curves for purified PHB, PHB8V, and PHBHx samples cooled from melt at different cooling rates are shown in Figure 3. The detailed information obtained from the analysis of the DSC data is in Table I. For PHB, the final melting temperature (T_m^f) increased as well as peak melting temperature (T_m^p), with a decrease in cooling rate, but the onset melting temperature (T_m^{onset}) did not change significantly, which suggests that the cooling rate influences the

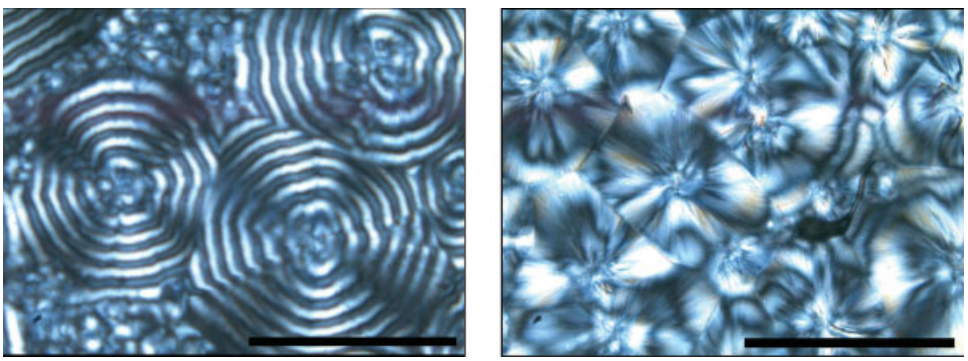

Figure 2 Polarized optical micrographs of PHB (as received) (left) and PHB (purified) (right) cooled from melt at 50°C/min. The scale bars equal to 100 μm. [Color figure can be viewed in the online issue, which is available at www.interscience.wiley.com.]

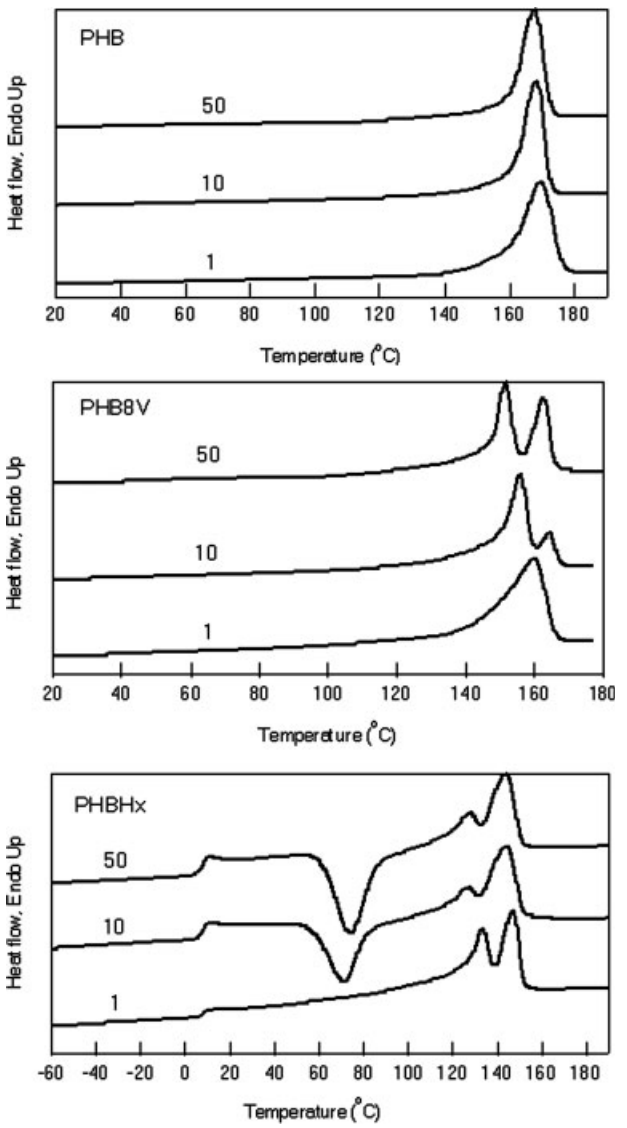

Figure 3 DSC curves for PHB, PHB8V, and PHBHx samples cooled from melt at 1, 10, and 50°C/min.

size and perfection of the first formed crystals to a great extent; whereas the cooling rate does not influence the crystals that form at later times and lower temperatures. For PHB8V, double melting peaks were observed at moderate to fast cooling rates (10–50°C/min), but a broad single peak was observed at slow cooling rate (1°C/min). As the cooling rate was decreased, the higher temperature peak area decreased while the lower temperature peak area increased, indicating that the higher melting peak is caused by the rearrangement of initial crystal morphology and that the lower melting peak represents the melting of original crystals formed when the sample was cooled from melt. This mechanism of melting, recrystallization, and remelting was verified by running DSC for PHB8V samples (50°C/min cooling rate) with different heating rates (data not shown here). The lower melting peak position shifted to higher temperature with a decrease in cooling rate, suggesting that the thickness of initial crystalline lamellae increases with a decrease in cooling rate. For PHBHx, double melting peaks were observed for all the cooling rates studied, which can also be explained by melting, recrystallization, and remelting process during heating.[13] In addition, the glass transition temperatures (T_g's), which were about 5°C for all samples were obtained from the midpoint of heat capacity change. PHBHx could crystallize from the melt during DSC cooling run at a slow cooling rate (for example 1°C/min), and thus cold crystallization of PHBHx were not observed at this condition. But when the cooling rate was increased (for example 10 and 50°C/min), cold crystallization peak was found after the glass transition of PHBHx during the following heating run, indicating that the crystallization rate of PHBHx was much slower than those of PHBV and PHB. The cold crystallization temperatures (T_{cc}'s) were 71.9 and 75.0°C and the enthalpies of cold crystallization (ΔH_{cc}'s) were 33.6 and 44.9 J/g for PHBHx samples cooled from melt with 10 and 50°C/min, respectively.

The crystallinities (X_c) of both PHB and PHB8V were very high (>60%), which leads to the brittleness of PHB and PHBV. The X_c increased with a decrease in cooling rate. The effect of cooling rates on X_c makes sense because at lower cooling rate macromolecules theoretically have more time for

TABLE I
Thermal Properties of PHB, PHB8V, and PHBHx Samples Cooled from Melt at 1, 10, and 50°C/min Obtained from Analysis of DSC Data

Samples (°C/min)	T_m^p(°C)	T_m^{onset}(°C)	T_m^f(°C)	ΔH_m (J/g)	X_c (%)
PHB 50	167.7	159.9	172.8	108.1	74
PHB 10	168.2	160.9	173.0	113.2	78
PHB 1	169.5	158.8	176.8	126.0	86
PHB8V 50	151.6, 162.6	147.0	166.1	75.2	69
PHB8V 10	155.9, 164.6	149.5	167.5	78.2	72
PHB8V 1	159.9	143.5	166.1	90.3	83
PHBHx 50	127.8, 144.3	119.4	151.1	44.5	39
PHBHx 10	127.4, 144.7	118.4	151.6	47.5	41
PHBHx 1	133.5, 147.4	127.4	152.0	54.8	48

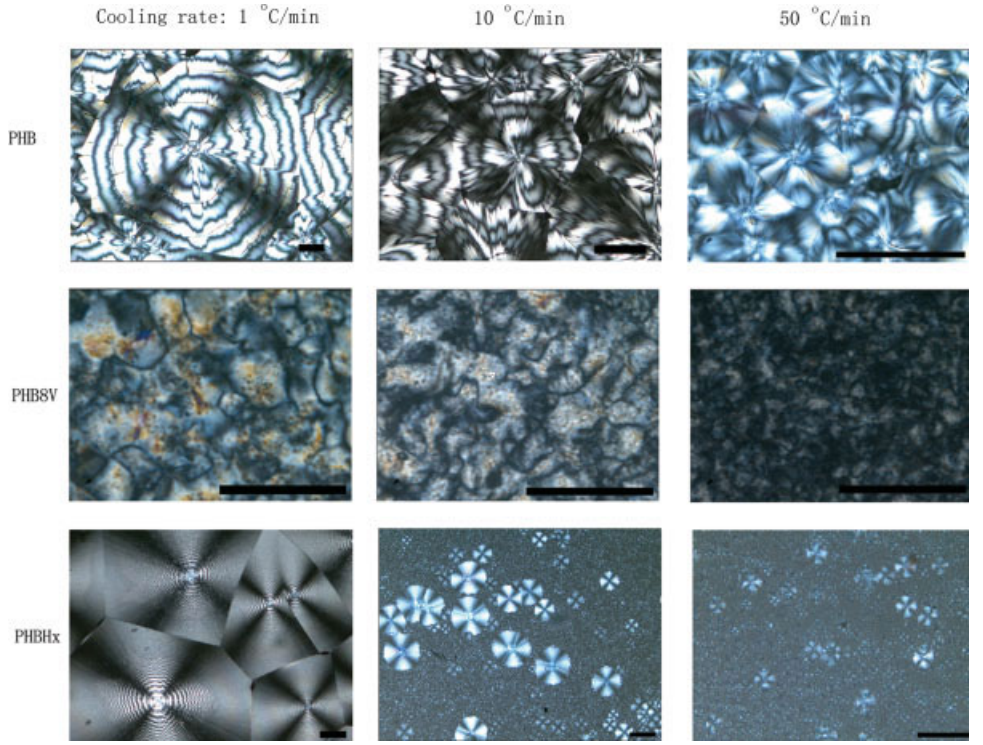

Figure 4 Polarized optical micrographs of PHB (scale bar = 100 μm), PHB8V (scale bar = 50 μm) and PHBHx (scale bar = 100 μm) samples cooled from melt at 1, 10, and 50°C/min. [Color figure can be viewed in the online issue, which is available at www.interscience.wiley.com.]

crystallization, which would result in fewer defects and thus higher X_c.[18]

Polarized optical micrographs of PHB, PHB8V, and PHBHx samples cooled from melt at different cooling rates are shown in Figure 4. For all samples studied, the size of the spherulites decreased when the cooling rate increased. The size of spherulites for PHB8V was always much smaller than that for PHB. At slow cooling rates (e.g., 1°C/min), both PHB and PHBHx had banded spherulites, indicating that lamellar twisting exists. When the cooling rate was increased to 50°C/min, the banded structure disappeared for spherulites of PHB. For PHB8V, the spherulitic textures were more disordered than those of PHB at a given cooling rate. At 10 and 50°C/min cooling rates, the size distributions of spherulites for PHBHx were very broad. The fact that at 1°C/min cooling rate, both PHB and PHBHx had banded spherulites, while PHB8V sample had nonbanded spherulites and more disordered textures infers that HHx comonomer is excluded from the HB crystal lattice, but the HV comonomer is incorporated into the HB crystal lattice, which leads to looser helical structures.[4] Because of the inclusion of HV comonomer and the highest cooling rate, PHB8V sample cooled from melt at 50°C/min cooling rate had very low birefringence, leading to a very poor contrast. The band spacing of PHB cooled from melt at 1°C/min was about 100 μm, which is close to that of PHB isothermally crystallized at 140°C.[39] The band spacing of PHB cooled from melt varied with the cooling rates, the spacing being larger at slower cooling rate (lower degree of supercooling) and becoming increasing smaller as the cooling rate was increased (higher degree of supercooling), which is consistent with the results found for polyethylene[40] and for PHB and PHBV.[41] When the cooling rate was increased to 50°C/min, the banded structure of PHB disappeared. However, we did not find banded spherulites for purified PHB8V samples, which is contrary to earlier results by Scandola et al.[41] and Gunaratne and Shanks.[10] Scandola et al. used ''as received'' samples for isothermal crystallization measurements, and Gunaratne and Shanks used only filtration to purify the samples. The mechanism put forward by Keith and Padden[42] to account for spherulitic type growth in both polymers and nonpolymers postulates a central role for impurities in the melt. Therefore, we propose that this discrepancy may be caused by impurities.

It has been well understood that isotactic polypropylene (iPP) form different types of spherulites, depending on the crystallization conditions. Several studies showed that different types of spherulites are caused by different crystalline forms.[37] In this study, WAXS was used to study the crystal structures of PHAs. The WAXS data for PHB, PHB8V, and PHBHx are shown in Figure 5.

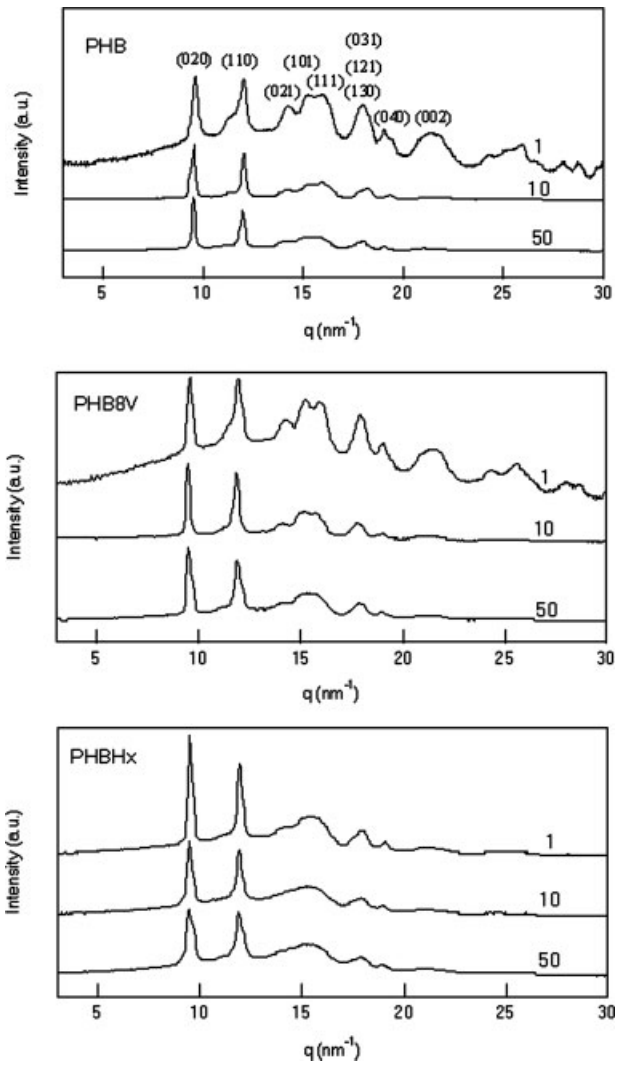

Figure 5 WAXS curves of PHB, PHB8V, and PHBHx cooled from melt at 1, 10, and 50°C/min.

The wide angle X-ray scattering data showed that PHAs studied had the same crystal structures, indicating that cooling rates have little influence on the crystal structures. Therefore, polymorphism is not one of the factors that lead to multiple melting peaks.

TABLE II
The *d* Spacings of the (110) and (020) Reflections, and the Lattice Parameters of *a* and *b* of PHB, PHB8V, and PHBHx Samples Cooled from Melt at 1, 10, and 50°C/min Obtained from Analysis of WAXS data

Sample (°C/min)	d_{110} (Å)	d_{020} (Å)	*a* (Å)	*b* (Å)
PHB 50	5.23	6.59	5.70	13.17
PHB 10	5.23	6.53	5.71	13.06
PHB 1	5.22	6.53	5.70	13.05
PHB8V 50	5.27	6.60	5.75	13.20
PHB8V 10	5.30	6.64	5.78	13.27
PHB8V 1	5.26	6.57	5.74	13.14
PHBHx 50	5.26	6.61	5.74	13.21
PHBHx 10	5.27	6.61	5.74	13.22
PHBHx 1	5.25	6.59	5.73	13.18

The unit cells of PHB, PHBV with less than 37 mol % HV, and PHBHx with less than 25 mol % HHx belong to the orthorhombic system, $P2_12_12_1$ (D_2^4) ($\alpha = \beta = \gamma = 90°$), with $a = 5.76$ Å, $b = 13.20$ Å, and $c = 5.96$ Å (fiber repeat).[24,43–46] The (110) and (020) peaks were fitted by the method introduced by Sato et al.[44] The detailed information obtained from the analysis of the WAXS data is in Table II. The (110) and (020) *d* spacings and the *a* and *b* lattice parameters of PHB8V and PHBHx were larger than those of PHB, indicating that the side chain of the HV and HHx units cause expansion in both directions of the plane perpendicular to the chain axis (i.e., the *ab* plane).[41] The *a* lattice parameter of PHBHx was always smaller than that of PHB8V at a given cooling rate, indicating that the propyl side chain of HHx has stronger inter- and intramolecular interactions than the ethyl side chain of HV, since the propyl side chain is located

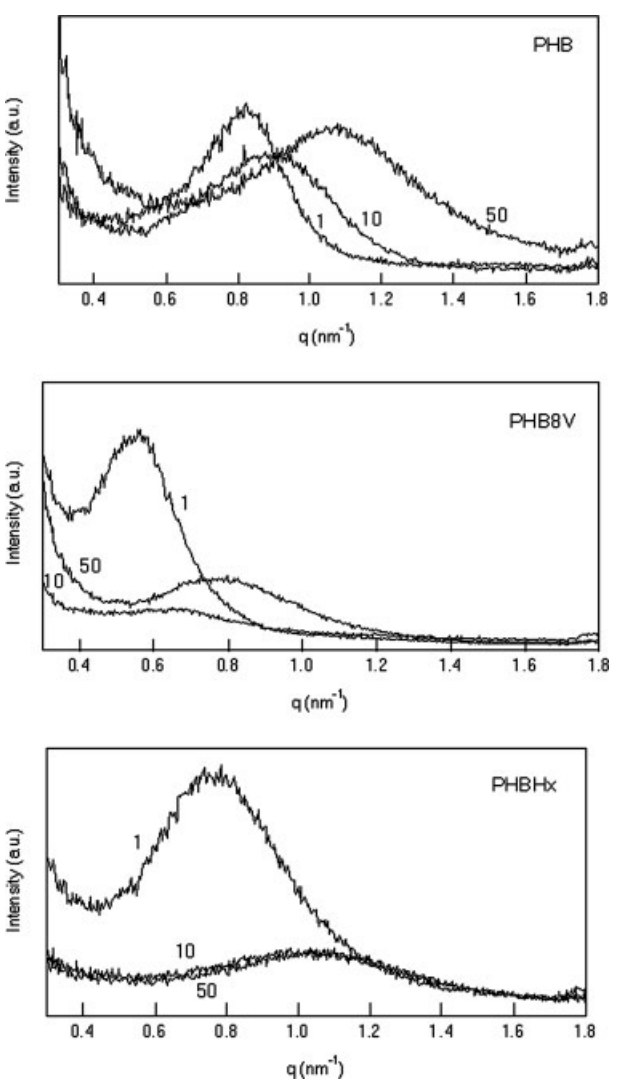

Figure 6 SAXS curves of PHB, PHB8V, and PHBHx cooled from melt at 1, 10, and 50°C/min (obtained from UMass Amherst).

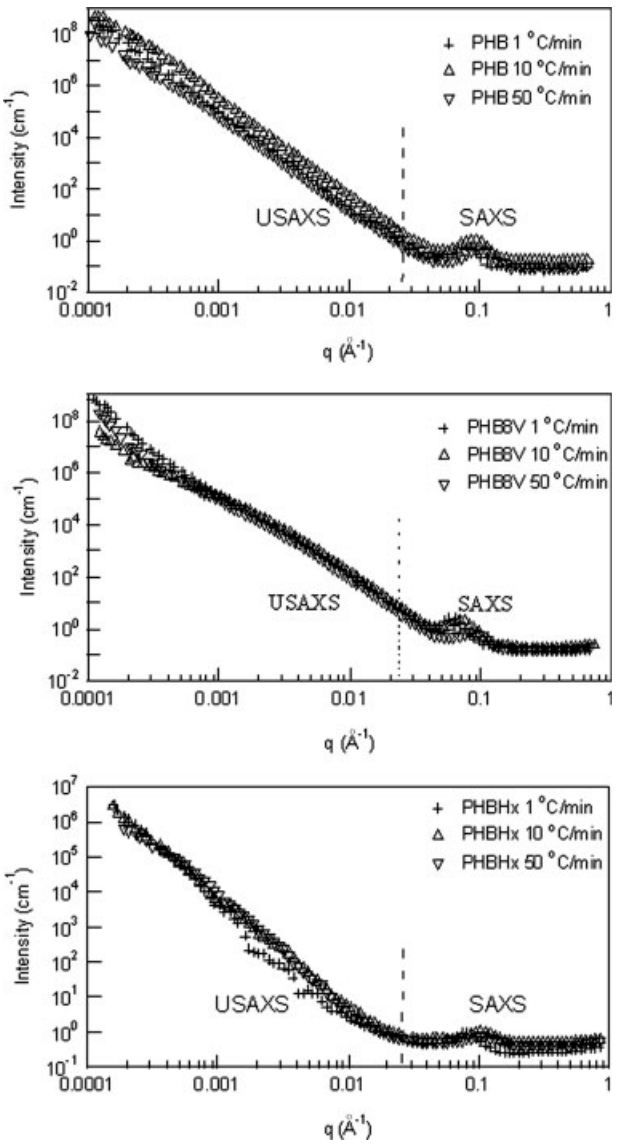

Figure 7 Intensity as a function of q for PHB, PHB8V, and PHBHx samples cooled from melt at 1, 10, and 50°C/min (obtained from APS at ANL).

closer to the C=O group in the lattice constant a axis than the ethyl side chain so that the C—H...O=C hydrogen bonding is stronger.[45] Another possibility is that the propyl side chains of HHx are protruded in the crystal structure, while the ethyl side chain of HV can be fixed in the crystal with PHB.[44]

Our results indicated that the cooling rates affect the spherulitic morphologies and does not influence the crystal structures. This motivated us to study the internal structures (lamellar and fibrillar structures) of the PHA spherulites. At smaller scattering angles, USAXS and SAXS can provide information on the internal structures of PHA spherulites. The SAXS data from UMass Amherst are shown in Figure 6, and the simultaneous USAXS/SAXS data are shown in Figure 7. Average values of lamellar morphological parameters obtained from UMass Amherst and from Argonne National Laboratory are listed in Table III. It was found that the long period (L) and average lamellar thickness (l_c) increased with decreasing cooling rate for PHB, PHB8V, and PHBHx, and that the L and l_c of PHB8V were always larger than those of PHB and PHBHx at a given cooling rate, whereas the L and l_c of PHBHx were smaller than those of PHB. These results suggest that HHx comonomer is excluded from the HB crystal lattice, but the HV comonomer is incorporated into the HB crystal lattice, which is consistent with previous work.[34,41,47]

TABLE III
The Average Values of Lamellar Parameters Obtained from Analysis of the SAXS Data of PHB, PHB8V, and PHBHx Samples Cooled from Melt at 1, 10, and 50°C/min Obtained from APS at Argonne National Laboratory and UMass Amherst

Samples (°C/min)	L (nm)	l_a (nm)	l_c (nm)
PHB 50	5.6 ± 0.3	2.8 ± 0.3	2.8 ± 0.1
PHB 10	6.3 ± 0.1	3.1 ± 0.1	3.2 ± 0.1
PHB 1	7.2 ± 0.1	3.6 ± 0.1	3.6 ± 0.1
PHB8V 50	6.4 ± 0.3	2.9 ± 0.2	3.5 ± 0.2
PHB8V 10	7.9 ± 0.3	3.5 ± 0.2	4.4 ± 0.1
PHB8V 1	10.1 ± 0.2	3.6 ± 0.2	6.5 ± 0.1
PHBHx 50	4.9 ± 0.4	2.8 ± 0.3	2.1 ± 0.2
PHBHx 10	5.1 ± 0.3	2.9 ± 0.2	2.2 ± 0.2
PHBHx 1	6.7 ± 0.2	3.1 ± 0.1	3.6 ± 0.2

The ± values denote the standard deviation.

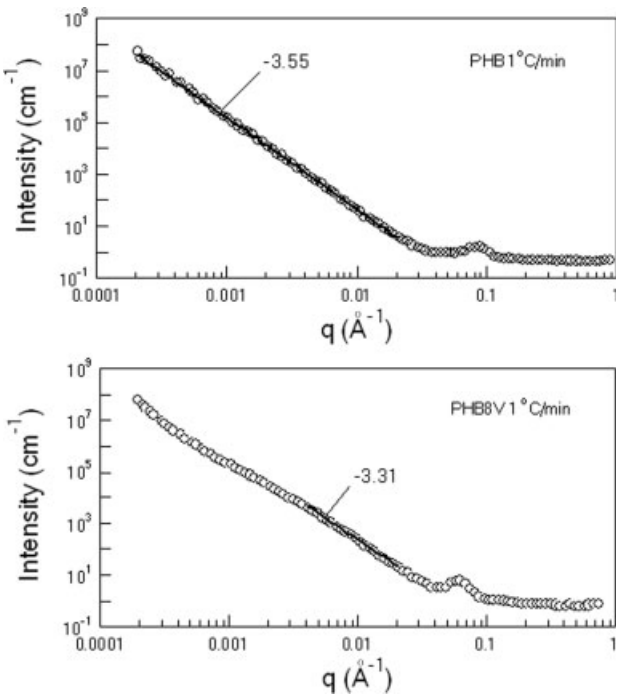

Figure 8 Intensity as a function of q for PHB and PHB8V samples cooled from melt at 1°C/min and the fitting curves from 0.00055 to 0.0200 $Å^{-1}$ and from 0.0040 to 0.0200 $Å^{-1}$ for PHB and PHB8V, respectively.

TABLE IV
The Limiting Slopes Obtained from the USAXS Region for PHB, PHB8V, and PHBHx Samples Cooled from Melt at 1, 10, and 50°C/min

Samples (°C/min)	Slope
PHB 50	−3.4 ± 0.2
PHB 10	−3.8 ± 0.1
PHB 1	−3.6 ± 0.1
PHB8V 50	−3.2 ± 0.2
PHB8V 10	−3.3 ± 0.2
PHB8V 1	−3.3 ± 0.1
PHBHx 50	−3.4 ± 0.3
PHBHx 10	−3.2 ± 0.2
PHBHx 1	−3.5 ± 0.1

The ± values denote the standard deviation.

On the basis of the polarized optical microscopy results shown in Figure 4, the size of PHB, PHB8V, and PHBHx spherulites was greater than 50, 2, and 10 μm, respectively. So the corresponding q value ($q = 2\pi/D$, where D is the diameter of the spherulite) was smaller than 1.3×10^{-5} Å^{-1}, 3.1×10^{-4} Å^{-1} and 6.3×10^{-5} Å^{-1} for PHB, PHB8V, and PHBHx, respectively. X-ray scattering arising from different spherulites (interparticle scattering) would contribute intensity chiefly at scattering vectors in the region of $q < 1.3 \times 10^{-5}$ Å^{-1}, $q < 3.1 \times 10^{-4}$ Å^{-1} and $q < 6.3 \times 10^{-5}$ Å^{-1} for PHB, PHB8V, and PHBHx, respectively. Therefore, scattering observed in these regions where the limiting slopes were obtained (from 0.00055 to 0.0200 Å^{-1}, from 0.0040 to 0.0200 Å^{-1} and from 0.00055 to 0.0200 Å^{-1} for PHB, PHB8V, and PHBHx, respectively) must originate from scattering within the spherulites. For PHB8V samples, interparticle scattering of spherulites 2–6 μm in size was observed at $q < 3.1 \times 10^{-4}$ Å^{-1}. Two examples showing how the limiting slopes were obtained are shown in Figure 8. The limiting slopes obtained for PHB, PHB8V, and PHBHx are listed in Table IV. For self-similar or fractal objects, it is well known that the scattered intensity $I(q)$ follows a power law, $I(q) \sim q^{-d}$, where d is a fractal dimension. For mass fractals, $1 < d < 3$, while for surface fractals $3 < d < 4$.[48,49] It must be noted that if the particle size distribution itself follows a power-law behavior, the scattering intensity will also exhibit similar power-law scaling and, invariably for such systems, d has been observed to fall in the range of from 3 to 4.[50] The fact that the limiting slopes for PHB, PHB8V, and PHBHx were all between −3 and −4 suggested that the aggregates of fibrils possess a surface that is rough or the size distribution of the aggregates of fibrils are polydisperse.

CONCLUSIONS

The influence of cooling rate on thermal behavior and morphologies of PHB, PHB8V, and PHBHx were investigated. It was found that the thermal behavior and morphologies of PHAs studied were observed to strongly depend on cooling rate. If impurities are present, multiple melting peaks of PHAs can be due to both melting, recrystallization, and remelting process and impurities. The long period (L) and average lamellar thickness (l_c) increased with decreasing cooling rate for PHB, PHB8V, and PHBHx. The lamellar morphology reflects that HHx comonomer is excluded from the HB crystal lattice, but the HV comonomer is incorporated into the HB crystal lattice. The size of the spherulites of PHAs studied decreased when the cooling rate increased. The WAXS pattern of the PHB, PHB8V, and PHBHx studied at room temperature showed that they all have an orthorhombic system, $P2_12_12_1$ (D_2^4) ($\alpha = \beta = \gamma = 90°$), with $a = 5.76$ Å, $b = 13.20$ Å, and $c = 5.96$ Å (fiber repeat), which is identical to that of the PHB crystal system. There was little influence of cooling rate on the crystal structures.

References

1. Madison, L. L.; Huisman, G. W. Microbiol Mol Biol Rev 1999, 63, 21.
2. Anderson, A. J.; Dawes, E. A. Microbiol Rev 1990, 54, 450.
3. Smith, R. Biodegradable Polymers for Industrial Applications; CRC Press LLC: Boca Raton, 2005.
4. Sato, H.; Dybal, J.; Murakami, R.; Noda, I.; Ozaki, Y. J Mol Struct 2005, 35, 744.
5. www.metabolix.com.
6. Grassie, N.; Murray, E. J.; Holmes, P. A. Polym Degrad Stab 1984, 6, 47.
7. Grassie, N.; Murray, E. J.; Holmes, P. A. Polym Degrad Stab 1984, 6, 95.
8. Grassie, N.; Murray, E. J.; Holmes, P. A. Polym Degrad Stab 1984, 6, 127.
9. Saad, G. R.; Seliger, H. Polym Degrad Stab 2004, 83, 101.
10. Gunaratne, L. M. W. K.; Shanks, R. A. Eur Polym J 2005, 41, 2980.
11. Erceg, M.; Kovacic, T.; Klaric, I. Polym Degrad Stab 2005, 90, 86.
12. Zini, E.; Focarete, M. L.; Noda, I.; Scandola, M. Compos Sci Technol 2007, 67 2085.
13. Abe, H.; Doi, Y.; Aoki, H.; Akehata, T. Macromolecules 1998, 31, 1791.
14. Iwata, T.; Tsunoda, K.; Aoyagi, Y.; Kusaka, S.; Yonezawa, N.; Doi, Y. Polym Degrad Stab 2003, 79, 217.
15. He, J.-D.; Cheung, M. K.; Yu, P. H.; Chen, G.-Q. J Appl Polym Sci 2001, 82, 90.
16. Bergmann, A.; Owen, A. Polym Int 2003, 52, 1145.
17. Wang, X.; Peng, S.; Dong, L. Colloid Polym Sci 2005, 284, 167.
18. Erceg, M.; Kovacic, T.; Klaric, I. Polym Degrad Stab 2005, 90, 313.
19. Li, Y.; Akpalu, Y. A. Macromolecules 2004, 37, 7265.
20. Kalay, G.; Bevis, M. J. J Polym Sci Part B: Polym Phys 1997, 35, 241.
21. Kalay, G.; Bevis, M. J. J Polym Sci Part B: Polym Phys 1997, 35, 265.
22. Fischer, J. J.; Aoyagi, Y.; Enoki, M.; Doi, Y.; Iwata, T. Polym Degrad Stab 2004, 83, 453.
23. Iwata, T.; Doi, Y. Macromol Symp 2005, 224, 11.
24. Doi, Y.; Kitamura, S.; Abe, H. Macromolecules 1995, 28, 4822.

25. Gunaratne, L.; Shanks, R. A.; Amarasinghe, G. Thermochim Acta 2004, 423, 127.
26. McAiley, J.; O'Brien, C.; Bruce, D. AIChE Annu Meeting and Fall Showcase; Cincinnati, OH, 2005.
27. Spitalsky, Z.; Bleha, T. Macromol Biosci 2004, 4, 601.
28. Sheng, N.; Boyce, M. C.; Parks, D. M.; Rutledge, G. C.; Abes, J. I.; Cohen, R. E. Polymer 2004, 45, 487.
29. Zhao, Q.; Cheng, G. X.; Song, C. J.; Zeng, Y.; Tao, H.; Zhang, L. G. Polym Degrad Stab 2006, 91, 1240.
30. Zhao, Q.; Cheng, G. X.; Li, H. M.; Ma, X. L.; Zhang, L. G. Polymer 2005, 46, 10561.
31. Huang, H.; Hu, Y.; Zhang, J. M.; Sato, H.; Zhang, H. T.; Noda, I.; Ozaki, Y. J Phys Chem B 2005, 109, 19175.
32. Zhang, L. L.; Goh, S. H.; Lee, S. Y.; Hee, G. R. Polymer 2000, 41, 1429.
33. Scandola, M.; Focarete, M. L.; Adamus, G.; Sikorska, W.; Baranowska, I.; Swierczek, S.; Gnatowski, M.; Kowalczuk, M.; Jedlinski, Z. Macromolecules 1997, 30, 2568.
34. Murthy, N. S.; Akkapeddi, M. K.; Orts, W. J. Macromolecules 1998, 31, 142.
35. Wang, Z. G.; Hsiao, B. S.; Murthy, N. S. J Appl Crystallogr 2000, 33, 690.
36. Gan, Z.; Abe, H.; Doi, Y. Biomacromolecules 2000, 1, 704.
37. Hemsley, D. A. Applied Polymer Light Microscopy; Elsevier Applied Science: New York, 1989.
38. Low, A.; Vesely, D.; Allan, P.; Bevis, M. J Mater Sci 1978, 13, 711.
39. Gazzano, M.; Focarete, M. L.; Riekel, C.; Scandola, M. Biomacromolecules 2000, 1, 604.
40. Lindenmeyer, P. H.; Holland, V. F. J Appl Phys 1964, 35, 55.
41. Scandola, M.; Ceccorulli, G.; Pizzoli, M.; Gazzano, M. Macromolecules 1992, 25, 1405.
42. Keith, H. D.; Padden, F. J., Jr. J Appl Phys 1963, 34, 2409.
43. Yokouchi, M.; Chatani, Y.; Tadokoro, H.; Teranishi, K.; Tani, H. Polymer 1973, 14, 267.
44. Sato, H.; Nakamura, M.; Padermshoke, A.; Yamaguchi, H.; Terauchi, H.; Ekgasit, S.; Noda, I.; Ozaki, Y. Macromolecules 2004, 37, 3763.
45. Sato, H.; Mori, K.; Murakami, R.; Ando, Y.; Takahashi, I.; Zhang, J.; Terauchi, H.; Hirose, F.; Senda, K.; Tashiro, K.; Noda, I.; Ozaki, Y. Macromolecules 2006, 39, 1525.
46. Allegra, G.; Marchessault, R. H.; Bloembergen, S. J Polym Sci Part B: Polym Phys 1992, 30, 809.
47. Bluhm, T. L.; Hamer, G. K.; Marchessault, R. H.; Fyfe, C. A.; Veregin, R. P. Macromolecules 1986, 19, 2871.
48. Owen, A.; Bergmann, A. Polym Int 2004, 53, 12.
49. Roe, R.-J. Methods of X-Ray and Neutron Scattering in Polymer Science; Oxford University Press: Oxford, UK, 2000.
50. Gheorghiu, S.; Coppens, M. O. Proc Natl Acad Sci USA 2004, 101, 15852.